scientific reports

Check for updates

OPEN

Effect of temperature on permeability of mudstone subjected to triaxial stresses and its application

Jieqing Yu[1], Fuke Dong[1]✉, Yu Zhou[1], Xingyan Wang[2], Liang Zhang[3] & Hailong Su[4]

In order to prevent leakage of pyrolysed oil and gas and the release of contaminants from the top and bottom strata, it is essential to carry out a comprehensive study of the seepage behaviour of these strata under high temperature triaxial stress conditions. The findings of this study will contribute to the development of effective strategies for the containment and integrity monitoring of subsurface reservoirs and storage environments. Mudstone, serving as both the upper and lower strata, offers an effective barrier due to its inherently low permeability. In order to explore the change rule of mudstone sealing performance under high temperature triaxial stress, an air-heated low permeability rock mass air permeability measurement system is used to measure the ground stress buried 500 m deep and the temperature variation characteristics of mudstone permeability on the roof and floor of Jimsar oil shale in Xinjiang under 100 °C. It was found that the permeability of stressed mudstone decreased with the temperature rising up to 100 °C. The primary factor influencing the outcome was the thermal expansion of the mudstone. The magnitude of the drop value was contingent upon the triaxial stresses that could potentially be induced by the application of significant tensile forces, resulting in a relatively minor drop value. The average hydraulic radius of pore in the mudstone was also calculated, which also exhibited continuous reduction as heating up to 100 °C and the degree of reduction could reach 68%. The capacity, that prevent oil & gas and contaminant from moving cross strata as a barrier, would be strengthened when the mudstone strata from roof and floor experienced the temperature low than 100 °C. The barrier performance of mudstone as a pollutant migration barrier layer to gas pollutant migration during in-situ heat injection mining of oil shale was further evaluated.

Keywords Mudstone, High temperature, Permeability, Triaxial stresses

Mudstone typically forms the upper and lower layers in sedimentary deposits, and it is characterized by its low permeability. In projects such as geological deep burial disposal of nuclear waste, geo-logical storage of CO_2, high temperature to reduce viscous oil extraction, and underground gasification/pyrolysis mining of coal, mudstone can be used as a containment layer to stop the migration of nuclides, oil and gas leakage, and contaminants[1–3]. The permeability of mudstone stands as a critical parameter for governing fluid transport within these projects. It serves as a pivotal indicator of the long-term safety and stability of such endeavors.

Studies have shown that the permeability of mudstone at room temperature is affected by triaxial stress and pore pressure, that is, it decreases with the increase of effective stress[4–9]. Temperature also has a significant effect on the permeability of rocks. Related studies can be categorized into two primary aspects: Firstly, rock specimens are subjected to heating at various temperatures, followed by cooling to room temperature, after which permeability measurements are conducted. This type of permeability measurement is referred to as post-high-temperature permeability. Secondly, permeability measurements are carried out on rock specimens while they are exposed to high temperatures and maintained under a triaxial stress state. This type of permeability measurement is referred to as real-time high-temperature permeability. Rock permeability is of great importance to the development of geological resources and energy and geological environmental protection. For example, in high temperature viscosity reduction oil development, coal underground gasification/pyrolysis, geothermal resources development and other projects, the thermal rupture caused by high temperature can improve coal

[1]Hebei Vocational College of Resources and Environment, Shijiazhuang 050081, China. [2]Hebei Institute of Geological Survey, Shijiazhuang 050081, China. [3]Jinqiao Coal Mine, Jining 272200, China. [4]Huayuan Well Field Resource Development Co., Ltd, Jining 272200, China. ✉email: 310097761@qq.com

rock permeability, which is beneficial to improve the recovery rate of oil and gas and geothermal resources. In terms of deep geological disposal of nuclear waste, deep geological storage of CO_2, construction of gas storage and sealing of cap rock in high temperature resource exploitation projects, the increase of permeability induced by thermal fracture of rock will cause risks such as radionuclide and oil and gas leakage. The utilization of permeability assessment is essential for evaluating the long-term safety of these projects.

Considerable research has been dedicated to the permeability of rocks following exposure to high temperatures. Zhang et al.[10] concluded that the permeability increased by three orders of magnitude by heating granite to 900 °C and then cooling it in water. Jin et al.[11] measured the permeability of granite after heating to 800 °C and then cooling it naturally and found that the permeability continued to increase with increasing heating temperature. He et al.[12] concluded by measuring the permeability of granite after high temperature that that permeability is exponentially related to temperature. Chen et al.[13] investigated the characteristics of permeability changes of granite in Beishan after high temperature and also obtained that permeability increases exponentially with temperature. The permeability change of sandstone after high temperature is similar to that of granite, which increases exponentially with temperatures[14].

Due to technical limitations of high-temperature and high-pressure percolation test equipment, not many real-time permeability measurements under high-temperature tri-axial stress have been carried out. Summer et al.[15] measured the permeability change of Westerly granite under triaxial stress and high temperature at 400 °C and concluded that the permeability at 400 °C is 1–2 orders of magnitude higher than that at room temperature. Darot et al.[16] also measured the permeability of granite under high-temperature triaxial stress permeability and found that permeability decreased with increasing temperature from room temperature to 125 °C and increased with increasing temperature above 125 °C. Feng et al. measured the variation of permeability of Lu ash granite up to 500 °C using a self-developed large-size high-temperature and high-pressure rock mechanics test system and found low values of permeability below 300 °C despite varying trends of elevation and elevation, and above 300 °C, the permeability appeared to increase more than 10 times, and 300 °C was considered as the critical temperature for the sudden change of granite permeability[17]. Sun et al.[18] studied the effects of coupled temperature and pressure changes on the porosity, permeability and rock mechanical characteristics of deep shale, and found that high temperature has a significant influence on the sensitivity of porosity and permeability stress compared with the experiment of normal temperature and high confining pressure. Lv[19] found that when the temperature is high and the confining pressure is large, the shear effect has a certain effect on the increase of permeability. When the confining pressure is large, the heat transfer coefficient of shear fracture is more sensitive to the confining pressure. Li et al.[20] found that the high pressure pulse permeability is closer to the actual rock permeability under high temperature and high pressure formation environment than other permeability. Liu et al.[21] studied the effects of surfactant mass fraction, displacement rate, injection amount, boring time, permeability and fracture on dynamic imbibition effect. It is found that permeability, fracture and dynamic imbibition efficiency are positively correlated. Large-scale volumetric fracturing and acidizing are important factors to improve dynamic imbibition efficiency. Zhao[22,23] found that the hydrostatic stress has an obvious inhibitory effect on the permeability and thermal deformation of granite, and the greater the hydrostatic stress, the more obvious the inhibitory effect. Under triaxial hydrostatic pressure, there is a linear relationship between injection pressure and injection flow in granite fracture, and the equivalent opening and permeability of fracture decrease exponentially with the increase of normal stress. Wu et al.[24] adopted the pressure pulse method and took granite parent rock and backfill as the research object to study the effect of effective stress on the permeability of granite parent rock and backfill under two paths of changing confining pressure or pore pressure. Fazio et al.[25] conducted a simulation study on sandstone permeability at different depths and found that the complex changes among stress, pore pressure and temperature were the main reasons affecting permeabilityYin et al.[26] believe that reservoir construction carried out in granite filling at the later stage of fracture will greatly reduce construction cost, increase reservoir water-rock heat exchange area and improve heat exchange efficiency, providing new technology and theoretical thinking for geothermal exploitation of deep dry hot rock. Compared with normal temperature water fracturing, Wu et al.[27], low-rate steam injection failure is a slow ductile tensile failure process, and the fracture is asymmetrically expanded relative to the drilling hole, and its width is smaller than that of hydraulic fracturing. Payton et al.[28] studied the relationship of pore permeability in geological materials by digital method, and found that grain sphericity was positively correlated with permeability. Li et al.[29] studied the permeability water transport by using nuclear magnetic resonance method. It was found that the water phase mainly distributed in the macropore and mesoppore.

At present, the study of post-high temperature and real-time high temperature rock permeability mainly focuses on granite and sandstone. In projects like coal underground gasification/pyrolysis, oil sands/thick oil injection thermal mining, and oil shale in-situ injection thermal mining, where mudstone serves as both the upper and lower barriers, it plays a vital role in effectively impeding the inter-layer transport of oil, gas, and pollutants. This preventive measure ensures that these substances do not escape into the atmosphere, thereby averting potential environmental pollution issues. Therefore, the study of permeability of mudstone under high temperature triaxial stress is very important. However, very little research has been conducted in this area. In this paper, the self-built air-heated low-permeability rock mass gas permeability measurement system was used to study the evolution of permeability with temperature in the mudstone of the top and bottom plates of Jimsar oil shale in Xinjiang within 500 m buried depth and 100 °C. It provides a basis for the feasibility evaluation of mudstone as an oil-gas and pollutant barrier layer in the in-situ heat injection mining of oil shale.

Test methods and procedures

Test methods and procedures

The mudstone specimens were collected from the bottom slab of an oil shale open pit in Jimsar, Xinjiang, and preserved in the field by sealing wax and oxygen isolation. The specimens were processed into cylindrical

specimens with a diameter of 50 mm by a sand line cutting machine in the laboratory, and a total of four pieces, all of which were vertically laminated specimens. The rock samples used in the test are shown in Fig. 1.

Due to the extremely low permeability of the mudstone, the specimen length was averaged to 20 mm in order to shorten the seepage measurement time. The specimens were gray in their natural state with no cracks visible to the naked eye, and the mineral composition is shown in Table 1.

Test equipment

The very low permeability measuring instrument was designed based on the pressure pulse decay method of Brace (1968)[30] and the published algorithm of SPE (1997)[31]. Mudstones are categorized as highly impermeable rock formations, and as a result, the pressure pulse method is employed for assessing their permeability.

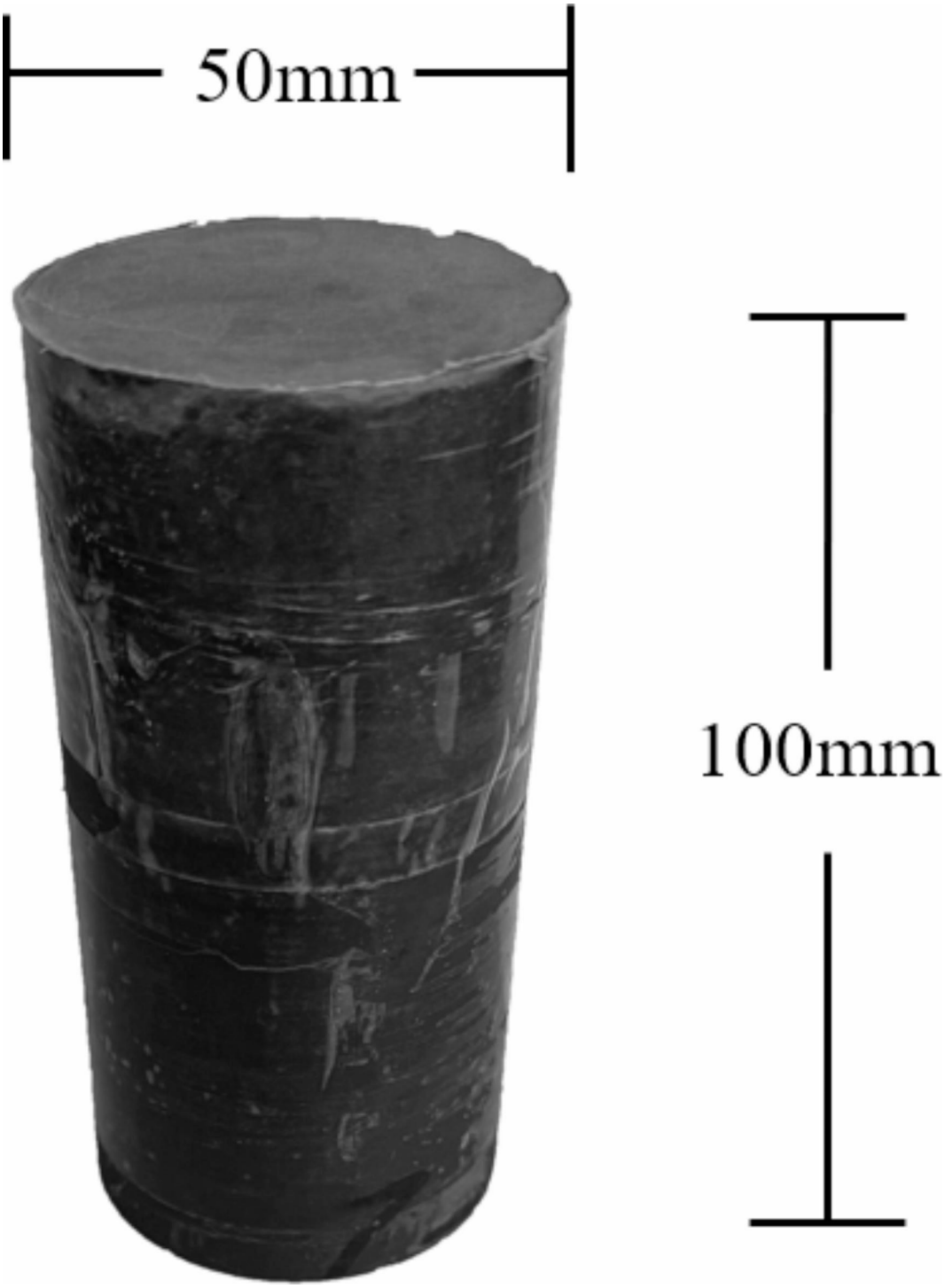

Fig. 1. Mudstone specimen.

Quartz	Plagioclase	Siderite	Clay minerals			
			Ima/ mono layer	Illite	Kaolinite	Turquoise
57%	10%	4%	23.78%	2.61%	2.32%	0.29%

Table 1. Mineral composition of mudstone.

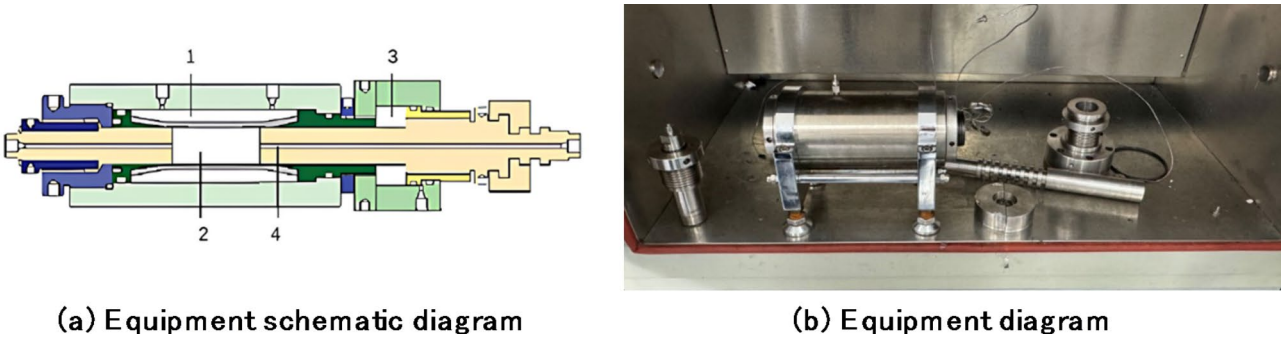

Fig. 2. This is a figure. Schemes follow the same formatting. (1. Circumferential pressure; 2. Specimen; 3. Axial pressure; 4. Pore pressure)

The pressure pulse method for measuring permeability is calculated by Eq. (1).

$$k = \frac{\mu\alpha\beta L V_1 V_2}{A(V_1 + V_2)} \tag{1}$$

Where, k is the specimen permeability, m^2; μ is the seepage medium dynamic viscosity, Pa s; β is the pore fluid compressibility coefficient, Pa^{-1}; A is the specimen cross-sectional area, m^2; L is the specimen length, m; V_1 is the upstream volume, m^3; V_2 is the downstream volume, m^3; α is the pressure decay coefficient, which is obtained from Eq. (2) by actual measurement.

$$\ln\left(\frac{p_1(t) - p_2(t)}{p_1 - p_2}\right) = -\alpha t \tag{2}$$

Where $P_1(t)$ is the upstream chamber pressure at any moment, Pa; $P_2(t)$ is the down-stream chamber pressure at any moment, Pa; P_1 is the initial upstream chamber pressure, Pa; P_2 is the initial downstream chamber pressure, Pa; t is the pressure decay time, s.

Figure 2 shows the structure of the test equipment for measuring the permeability of very low permeability rocks by the pressure pulse method, and the whole test system is placed in a constant temperature chamber. During the experiment, after loading the specimen into the rubber sleeve, in order to prevent the rubber sleeve from being sheared by the circumferential pressure, the axial pressure is loaded first, and then the circumferential pressure is loaded, both of which are loaded by liquid pressure transfer, and the high temperature resistant rubber sleeve is used to isolate the pore pressure from the circumferential pressure, and the heating method is thermostat air bath heating, and the temperature data of the specimen are measured and collected by thermocouples. Its pressure sensor model is PT124B-210 4-20MA, its reaction speed can reach 0.1s, accuracy can reach 0.01 kPa. The electric thermostat is YD-II, and the temperature range is 5 °C~200 °C.

Test procedure

The buried depth of oil shale in Jimsar, Xinjiang is less than 200 m. According to the average formation rock density of 2.5t / m^3, the axial pressure is set to 5 MPa in the test. Considering 1.2 times of the lateral pressure coefficient, the confining pressure is set to 6 MPa. The specific steps are as follows:

(1) After the specimens are prepared, measure the diameter and length of multiple groups, load the specimens into the test equipment shown in Fig. 1 according to the operation procedures, and connect the relevant pipelines.

(2) The specimens were loaded with an axial pressure of 5 MPa and a circumferential pressure of 6 MPa. The pressure was maintained and the permeability at different pore pressures was measured at room temperature with helium as the pore medium.

(3) Keep the axial pressure and the surrounding pressure constant, unload the pore pressure, and evacuate. The specimens were warmed up to 40 °C according to the heating rate of 7 °C/h and held for 4 h. Then keep the axial pressure, surrounding pressure and temperature constant, evacuate again, and measure the permeability at different pore pressures (2 MPa, 3 MPa, 4 MPa, 5 MPa).

(4) Following step (3), the permeability measurement at this target temperature was carried out by heating to the next target temperature at a heating rate of 7 °C/h. The target temperatures were 40 °C, 60 °C, 80 °C, and 100 °C, respectively.

In order to compare the effect of different ground stress conditions on permeability, a permeability measurement test was also conducted under ground stress conditions at 500 m burial depth, with the axial pressure set at 12.5 MPa and the surrounding pressure at 15 MPa. The target temperature was set as above and the measurement procedure was the same.

Test results and analysis

The permeability of a rock is a characterization of the ability of the rock to allow the passage of fluids and is an essential property of the rock, the magnitude of which is independent of the nature and type of fluid medium used for the measurement. However, extensive tests have found that for dense rocks, the permeability measured using a gas medium is significantly different from that measured using a liquid medium. The lower the permeability of the rock, the greater this discrepancy is due to the presence of the slip effect during gas measurements. The physical essence of the slip effect, also known as the Klinkenberg effect, is that when the average free range of the gas molecules is comparable to the pore size in the rock, the velocity of the gas movement on the pore wall is no longer zero, and therefore a slip flow is added to the measured gas flow rate, resulting in a higher gas measured permeability than the absolute permeability of the rock. In $19k_g = bk\frac{1}{P_g} + k41$, Klinken-berg L.J gave a correction for equation for the gas-measured permeability, namely:

$$k_g = k\left(1 + \frac{b}{P_g}\right) \tag{3}$$

Where: kg is the gas measured permeability, m^2; k is the absolute permeability, m^2; Pg is the average gas pressure, MPa; b is the Klinkenberg coefficient, which depends on temperature, gas type and pore structure and can be determined from Eq. (4)

$$b = \frac{4c}{r}\lambda P_g \tag{4}$$

Where: c is the scaling factor with a value of about 1; r is the average hydraulic radius of the pore, m; λ is the average free range of the gas molecules, m, which is calculated as follows:

$$\lambda = \frac{k_B T}{\sqrt{2}\pi d^2 P} \tag{5}$$

Where: k_B is Boltzman constant, 1.380649×10^{-23} J/K; T is temperature, K; d is molecular dynamics diameter of gas, 0.258×10^{-9}m for helium; P is gas pressure, MPa.

Rearranging Eq. (1), we can obtain Eq. (6) that:

$$k_g = bk\frac{1}{P_g} + k \tag{6}$$

It can be seen that the gas-measured permeability is linearly related to the inverse of the average gas pressure, and when the gas pressure is infinite, the gas-measured permeability is equal to the absolute permeability. By fitting the gas-measured permeability and the mean gas pressure inverse data, the intercept of the fitted line is the absolute permeability, and the Klinkenberg coefficient can be derived, and then the average hydraulic radius of the pore can be derived.

As shown in Fig. 3, the gas-measured permeability of the mudstone is extremely low in the order of 10–20 m^2 under both 200 m and 500 m ground stress conditions, and shows a significant linear relationship with the mean gas pressure inverse, indicating that the mudstone has a significant slip effect. By fitting the data in Fig. 4, the absolute permeability k and the Klinkenberg coefficient b of the mudstone at different temperatures can be obtained.

From Eq. (1), the permeability measurement results are related to the dynamic viscosity and compression coefficient of the pore fluid. In this paper, He is used as the pore fluid, which is considered to have no adsorption with the mudstone. By substituting the dynamic viscosity and compression coefficient of different temperatures and pressures into Eq. (1), the permeability of the mudstone at different temperatures and pore pressures can be obtained, i.e., the results in Fig. 2. Then the absolute permeability of mudstone after considering Klinkenberg effect is obtained by fitting the data in Fig. 3 according to Eq. (6), and its evolution law with temperature is shown in Fig. 4.

It can be seen from Fig. 3 that the permeability of the mudstone at room temperature is extremely low, 18.6×10^{-21} m^2, or 18.6nD, for 200 m burial depth ground stress conditions (i.e., $\sigma_a = 5$ MPa and $\sigma_c = 6$ MPa), which is generally lower than 10^{-15} m^2 as low permeability. With the increase of temperature, the increment is only 2.6nD, which is about 14%, although it increases slightly at 40 °C, which is not a significant increase. When the temperature increases further, the permeability continues to decrease to 1.75nD at 100 °C, which is only 9.4% of that at room temperature, a decrease of 1 order of magnitude. Com-pared with the 200 m burial depth ground stress condition, the permeability of mudstone under 500 m burial depth ground stress (i.e., $\sigma_a = 12.5$ MPa, $\sigma_c = 15$ MPa) condition is about 6.7 nD at room temperature, which is the result of the influence of triaxial pressure. The larger the triaxial pressure is, the larger the mudstone compression and deformation is, the mudstone pore closure and permeability decrease, which is also consistent with the general conclusion. Under the 500 m ground stress condition, the mudstone permeability shows a monotonic decrease with increasing

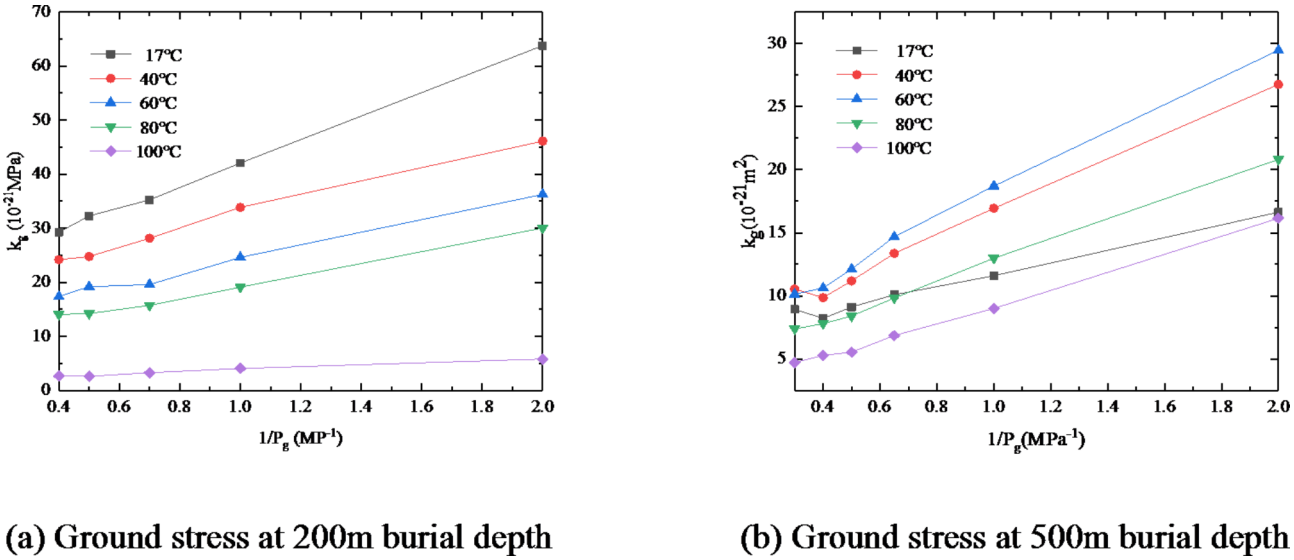

Fig. 3. Relationship between gas-measured permeability and the inverse of gas-averaged pressure.

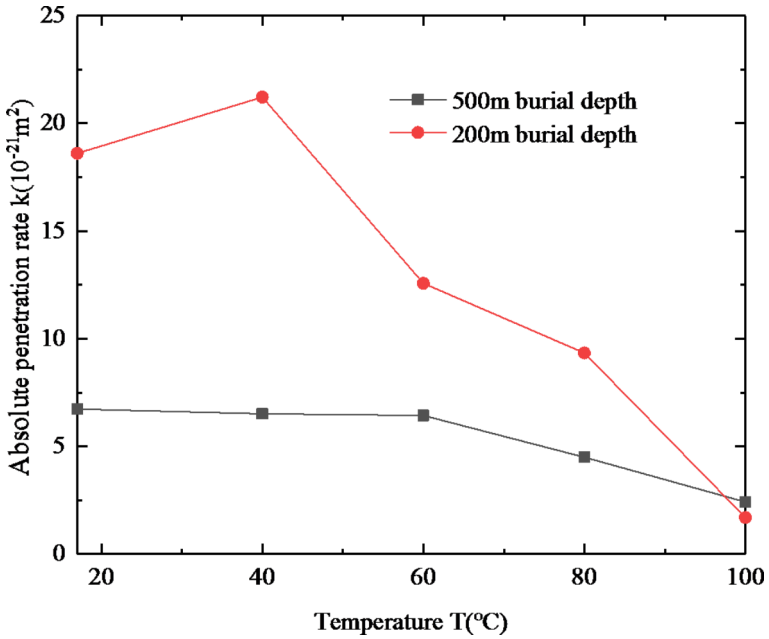

Fig. 4. Curve of absolute permeability of mudstone with temperature.

temperature to 2.3 nD at 100 °C, which is about 34% of that at room temperature. The reasons are as follows: with the increase of triaxial pressure, the cracks inside the specimen are closed, and the gas flow per unit time through the specimen is reduced, and its permeability is reduced. The specimen buried 500 m deep is affected by ground stress, and its internal fracture closure is greater than that of the specimen buried 200 m deep, so the permeability is also small.

The two curves in Fig. 4 are fitted to a straight line, and the slope indicates the value of permeability reduction per unit of temperature increase. the slopes for 200 m and 500 m burial depth conditions are −2.20 nD/10 °C and −0.52 nD/10 °C, respectively, and the negative sign indicates the decrease of permeability with increasing temperature. The significant difference between the two is mainly affected by the ground stress, and from the results, the higher the ground stress, the smaller the absolute value of the slope, and the mechanism is the same as above.

The permeability of mudstone is influenced by temperature in two contrasting ways: On one hand, at lower temperatures, thermal cracking in mudstone tends to be relatively weak, resulting in an increase in permeability. On the other hand, as temperatures rise, mudstone undergoes continuous thermal expansion deformation.

Under the influence of triaxial stress, microcracks and existing pores within the mudstone tend to close, leading to a reduction in permeability. In the low-temperature stage, the effect of permeability reduction induced by pore-fracture closure is significantly higher than that of permeability increase induced by thermal rupture; therefore, the mudstone integrally exhibits a permeability reduction.

Based on Eqs. (4) and (5), Eq. (7) is obtained as:

$$b = \frac{4ck_BT}{\sqrt{2}\pi d^2} \cdot \frac{1}{r} \tag{7}$$

Bringing in each known parameter in Eq. (7), the average hydraulic radius of the mudstone pore space at different temperatures can be obtained, as shown in Fig. 5.

As seen in Fig. 5, the pore hydraulic radius shows an overall decrease with in-creasing temperature, which is consistent with the trend of permeability change. The pore hydraulic radius of mudstone pore at room temperature was 72 nm (200 m burial depth ground stress condition specimen) and 74 nm (500 m burial depth ground stress condition specimen), which decreased to 57.5 nm and 23.7 nm at 100 ℃, with a decrease of about 20% and 68%, respectively. The pore hydraulic radius represents the average pore radius, which shows that the average pore size of mudstone decreases overall with increasing temperature, and the greater the triaxial stress, the greater the decrease, which is the essence of the decrease of mudstone permeability.

Evaluation of the effect of mudstone on the migration barrier of oil shale pyrolysis products

The conceptual model of oil shale formation is shown in Fig. 5, and the permeability of mudstone at high temperature is used to evaluate the effect of mudstone on the migration barrier of oil shale pyrolysis products. In

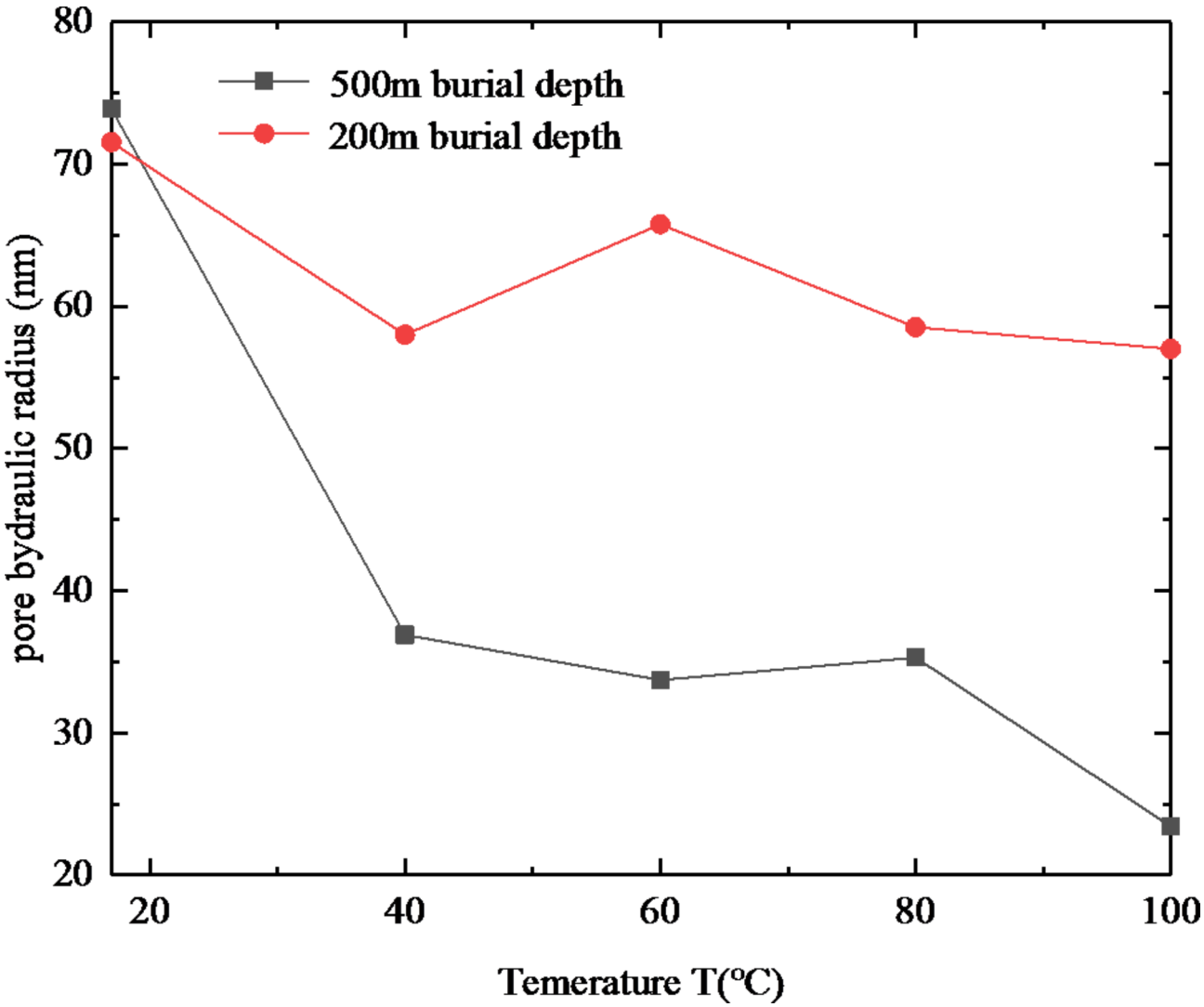

Fig. 5. Variation of pore hydraulic radius of mudstone at different temperatures.

Physical quantity	Oil shale	Mudstone	Shaly sandstone
Density kg/m^3	2400	2600	2700
Thermal conductivity W/(m K)	1.84	1.32	1.30
Specific heat capacity J/(kg K)	1500	1190	1010

Table 2. The basic parameters of each stratum in temperature calculation.

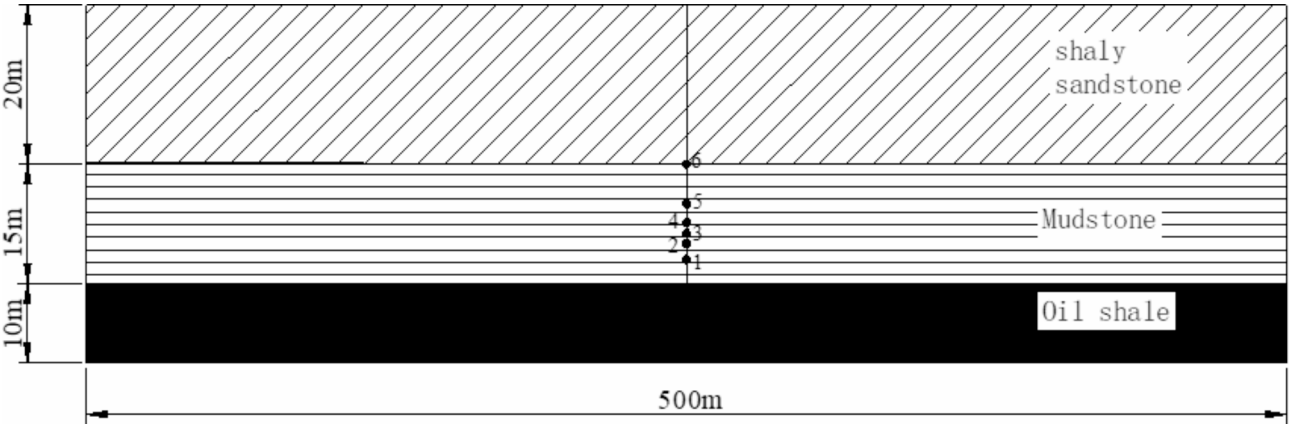

Fig. 6. The conceptual model of oil shale formation (numbers 1–6 represent temperature mon-itoring points, corresponding to 3 m, 5 m, 6 m, 7 m, 10 m and 15 m from the top surface of oil shale).

this model, the oil shale formation is 10 m thick, and above it is the mudstone formation and muddy sandstone formation with thicknesses of 15 m and 20 m. In the oil shale in-situ heat injection mining project, the oil shale formation is subjected to high temperature (600 °C), and heat conduction occurs between the top plate of the mudstone and the oil shale formation, and heat conduction is dominant in the mudstone formation, and the temperature distribution in the mudstone formation is calculated according to the one-dimensional heat conduction.

The physical parameters of each layer are summarized according to the previous study, as shown in Table 2[32]. It shows basic parameters, the initial formation temperature is 20 °C, and the horizontal dimension 500 m in the model indicates the distance between the heat injection well and the production well. The temperature variation with time at four location points 3 m (monitoring point 1), 5 m (monitoring point 2), 6 m (monitoring point 3), 7 m (monitoring point 4), 10 m (monitoring point 5) and 15 m (monitoring point 6) from the top surface of the oil shale formation is shown in Fig. 6.

It can be seen from Fig. 7 that the temperature of the mudstone layer 3 m away from the oil shale layer (monitoring point 1) continues to increase with the increase of heat injection mining time, reaching 100 ° C on the 55th day and 335 ° C on the 300th day. The change trend of mudstone temperature at 5 m away from oil shale layer (monitoring point 2) with heat injection mining time is the same as that at 3 m. By the 150th day of heat injection mining, the temperature has reached 100 °C, and it further escalates to 193 °C by the 300th day. On the 300th day following heat injection mining, the temperature at monitoring point 4 precisely reaches 100 °C. Meanwhile, at monitoring points 5 (10 m depth) and 6 (15 m depth), the temperatures do not exceed 50 °C. Specifically, the temperature at monitoring point 5 is recorded at 39.6 °C, while the temperature at monitoring point 6 remains nearly at its initial temperature.

According to the permeability values of mudstone at different temperatures obtained in Fig. 4, the barrier characteristics of caprock mudstone on the migration of pollutants after pyrolysis of oil shale formation are calculated and evaluated. There are two kinds of pollutants produced after pyrolysis of oil shale: gaseous (such as hydrocarbon gas produced by pyrolysis) and liquid (such as light oil). In terms of migration capacity, gas products are stronger than liquid products. Therefore, gas products are used to calculate the barrier capacity of mudstone. Assuming that the gas is CH_4, the gas pressure is 5 MPa, the density at 100 °C is $\rho = 26.64$ kg / m^3, and the dynamic viscosity is $\mu = 1.4 \times 10^{-5}$Pa · s. The permeability k of the mudstone obtained by the test is substituted into the Darcy 's law (Eq. 8), and the specific flow rate q of CH_4 flowing in the mudstone formation is obtained.

$$q = \frac{Q}{A} = \frac{k(P_1^2 - P_2^2)}{2\mu P_0 L} \tag{8}$$

In the formula, q is the specific flow, m/s; Q is gas flow, m^3/s; A is the cross-sectional area of the rock stratum through which the fluid passes. Here, the unit volume is taken, that is, the cross-sectional area is 1 m^2; L is the length of the rock layer through which the fluid passes, take 1 m, P_1 is the gas pressure at the inlet end, here set

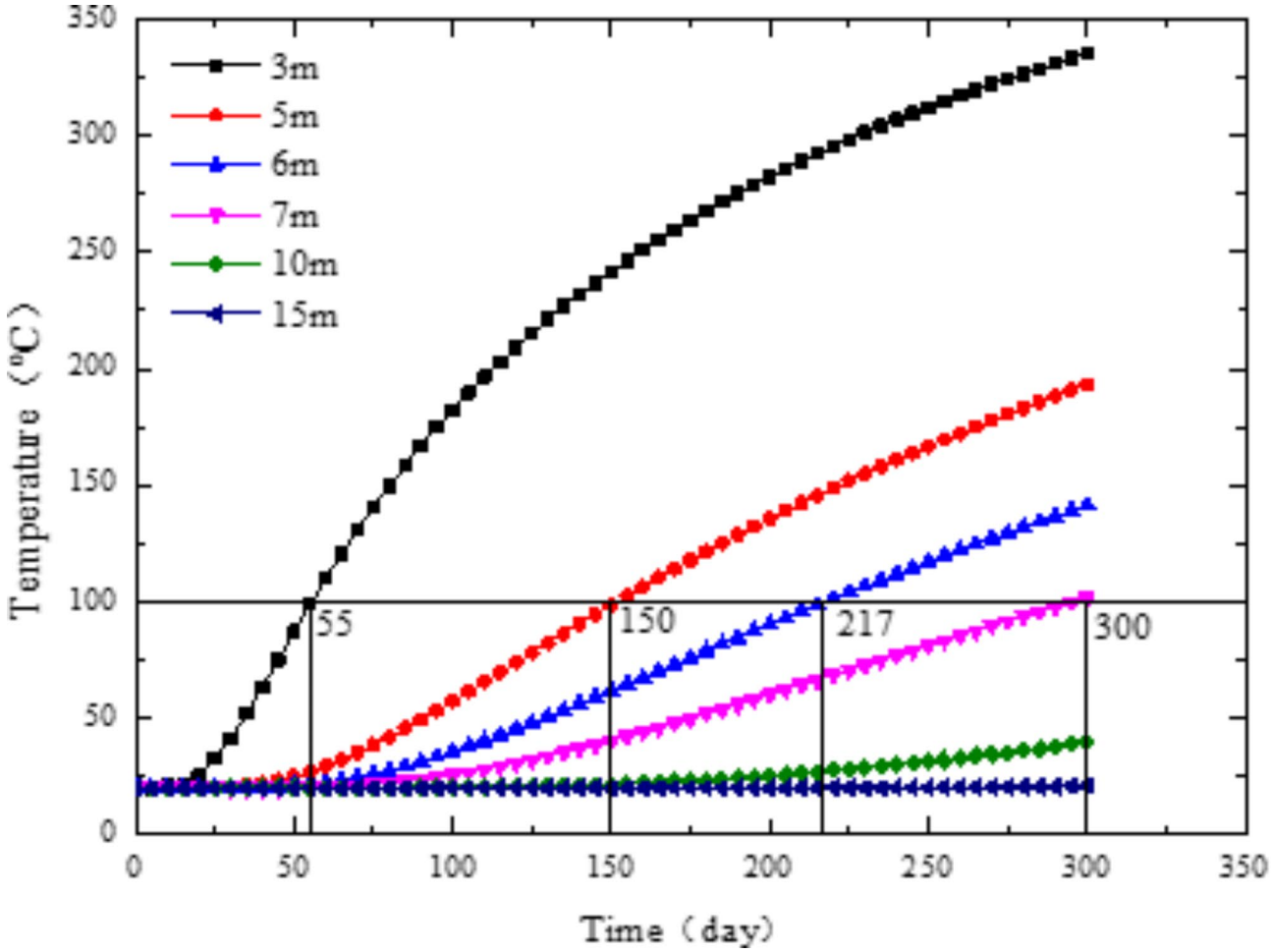

Fig. 7. The change law of measuring point temperature with time.

Temperature /℃	Penetration rate /$10^{-21}m^2$	Power Viscosity /10^{-5} Pa·s	specific flow /$10^{-8}m·s^{-1}$	Time spent per unit migration distance /day·m^{-1}
20	18.64	1.19	19.58	59
40	21.25	1.24	21.42	54
60	12.60	1.30	12.16	95
80	9.29	1.35	8.60	134
100	1.76	1.40	1.57	736

Table 3. Specific flow rate of methane transport in mudstone at different temperatures (200 m burial depth).

to 5 MPa, that is, $P_1 = 5$ MPa; P_2 is the gas pressure at the outlet end. Assuming that there is no gas in the original formation, it is set to 1 atmospheric pressure, that is, 0.1 MPa, that is, $P_2 = 0.1$ MPa; P_0 is atmospheric pressure, which is 0.1 MPa. The specific flow rate of CH_4 in mudstone at 200 m buried depth and different temperatures is calculated in Table 3.

According to the calculated specific flow rate, the time required to obtain the unit migration distance of CH_4 gas can be further calculated, as shown in Table 3. In the process of in-situ heat injection mining of oil shale, if the well spacing is 500 m, the mining time is calculated according to 300days. When the injection-production well is completed and the heat injection is stopped in this area, the temperature in the mudstone layer of the oil shale roof is 7 m away from the top of the oil shale layer. The temperature reaches 100 °C, and in the mudstone layer of more than 7 m, the temperature is less than 100 °C. According to Table 3, the unit migration distance of gaseous pollutants produced by pyrolysis of oil shale formation is time-consuming, and it takes 736days for gaseous pollutants to pass through 100 °C formation 1 m. Therefore, in the model mining process calculated in this paper, the pollutants almost do not pass through the mudstone formation. During the shutdown period, the pressure of gaseous pollutants in the oil shale formation decreases, the migration ability further decreases, and the possibility of crossing the mudstone layer is lower.

In summary, within 100 °C, the permeability of mudstone decreases with the increase of temperature, forming a barrier to block fluid migration, which has a good barrier effect on pollutant migration.

Conclusion

In order to investigate the real-time permeability evolution of mudstone, we employed our self-constructed air-heated low-permeability rock gas permeability measurement system. This study was conducted under specific conditions, including a ground stress level corresponding to a burial depth of 500 m and a temperature of 100 °C. The primary conclusions drawn from this research are as follows:

(1) At room temperature, the permeability of mudstone is markedly low, with a magnitude of 10–20 m^2. There is an overall trend of continuous decrease with increasing temperature, reaching 10–21 m^2 at 100 °C. It was observed that as ground stress increased, the magnitude of the decrease diminished. The primary factor influencing the reduction in permeability with increasing temperature is the thermal expansion of mudstone.

(2) A substantial Klinkenberg effect is observed in mudstone. Through the application of correction and data fitting techniques, a further law governing the pore hydraulic radius of mudstone as a function of temperature was obtained. This law states that the pore hydraulic radius decreases continuously with increasing temperature, with a maximum drop of up to 68%. This phenomenon is the underlying cause of the reduction in permeability observed in mudstone.

(3) From an engineering standpoint, the application of mudstone as a cover or bottom barrier is enhanced when its temperature is below 100 °C. This can effectively impede the trans-layer migration of oil and gas and contaminants during the in-situ thermal injection extraction of oil shale.

Data availability

The datasets used and/or analysed during the current study available from the corresponding author on reasonable request.

Received: 28 September 2023; Accepted: 12 November 2024
Published online: 19 November 2024

References

1. Feng, Z. J., Zhang, C., Dong, F. K. & Yang, D. Elastic modulus evolution of triaxially stressed mudstone at high temperature up to 400℃. *Energy Sci. Eng.* **8** (11), 4126–4135. https://doi.org/10.1002/ese3.801 (2020).
2. Feng, Z. J., Qiao, M. M., Dong, F. K., Yang, D. & Zhang, P. Thermal expansion of triaxially stressed mudstone at elevated temperatures up to 400℃. *Adv. Mat. Sci. Eng.* **2020**, 1–8. https://doi.org/10.1155/2020/8140739 (2020).
3. Luo, Z. S., Duan, Y. Z., Wang, X. W. & Zhang, X. S. Evaluation on sealing performance of mudstone caprocks of gas reservoir-type gas storage in high temperature environment. *China Saf. Sci. J.* **32** (2), 74–82. https://doi.org/10.16265/j.cnki.issn1003-3033.2022.02.011 (2022).
4. Zhang, Y., Yu, T. T., Zang, T., L, S. Y. & Zhou, J. W. Experimental study of the permeability evolution of fractured mudstone under complex stress paths. *Chin. J. Eng.* **43** (7), 903–914. 10.13374/j. issn2095-9389.2020.05.27.005 (2021).
5. Sun, Z. X. et al. Permeability stress sensitivity and gas-slippage effect of low-permeability porous media: An experimental case study of mudstone/shale of Chang 7 Member of Yanchang formation in the Ordos Basin. *Geochemic* **48** (6), 624–631. https://doi.org/10.19700/j.0379-1726.2019.06.010 (2019).
6. Fei, F. X. et al. Permeability variation of artificial fracture in Jimusaer Shale reservoir. *Sci. Technol. Eng.* **21** (20), 8329–8335 (2021).
7. Zang, T. J., Chen, G., Shang, H. B. & Shi, T. Triaxial seepage test of fractured mudstone and its stability analysis. *Coal Technol.*, **36** (12): 100–103. https://doi.org/10.13301/j.cnki.ct.2017.12.039 (2017).
8. Zeng, Z. J., Li, X. C., Shi, L. & Bai, B. Testing study on variational characteristics of the permeability for mudstone and sandstone with the change of confining pressure. *J. Transp. Sci. Eng.* **31** (4), 1–5. https://doi.org/10.16544/j.cnki.cn43-1494/u.2015.04.001 (2015).
9. Tian, Y. M., Tian, T. H., Xu, Y. D. & Chan, J. Stress sensitivity evaluation of shale reservoir of well Fanye-1 in Dongying sag. *Petrochem. Ind. Appl.*. **35** (4), 37–41 (2016).
10. Zhang, F., Zhao, J. J., Hu, D. W. & Skoczylas, J. F. Laboratory investigation on physical and mechanical properties of granite after heating and water-cooling treatment. *Rock. Mech. Rock. Eng.* **51**, 677–694. https://doi.org/10.1007/s00603-017-1350-8 (2018).
11. Jin, P. H. et al. Influence of different thermal cycling treatments on the physical, mechanical and transport properties of granite. *Geothermics* **78**, 118–128. https://doi.org/10.1016/j.geothermics.2018.12.008 (2019).
12. He, L. X., Yin, Q. & Jing, H. W. Laboratory investigation of granite permeability after high-temperature exposure. *Processes* **6** (36), 1–14. https://doi.org/10.3390/pr6040036 (2018).
13. Chen, S. W., Yang, C. H. & Wang, G. B. Evolution of thermal damage and permeability of Beishan granite. *Appl. Therm. Eng.* **110**, 1533–1542. https://doi.org/10.1016/j.applthermaleng.2016.09.075 (2017).
14. Yang, S. Q., Xu, P., Li, Y. B. & Huang, Y. H. Experimental investigation on triaxial mechanical and permeability behavior of sandstone after exposure to different high temperature treatments. *Geothermics* **69**, 93–109. https://doi.org/10.1016/j.geothermics.2017.04.009 (2017).
15. Summers, R., Winkler, K. & Byerlee, J. Permeability changes during the flow of water through westerly granite at temperatures of 100 ℃–400 ℃. *J. Geophys. Res.* **83** (B1), 339–344. https://doi.org/10.1029/JB083iB01p00339 (1978).
16. Darot, M., Gueguen, Y. & Baratin, M. L. Permeability of thermally cracked granite. *Geophys. Res. Lett.* **19** (9), 869–872. https://doi.org/10.1029/92GL00579 (1992).
17. Feng, Z. J., Zhao, Y. S., Zhang, Y. & Wen, Z. Real-time permeability evolution of thermally cracked granite at triaxial stresses. *Appl. Therm. Eng.* **133**, 194–200. https://doi.org/10.1016/j.applthermaleng.2018.01.037 (2018).
18. Sun, C. X. et al. Pore permeability and rock mechanics characteristics of the Longmaxi formation shale in deep Sichuan Basin under the coupling effect of temperature and pressure. *Pet. Explor. Dev.* **50** (01), 77–88. https://doi.org/10.11698/PED.2022023 (2023).
19. Lu, W. Study on seepage heat transfer characteristics of high temperature and high pressure single fracture granite. https://doi.org/10.27661/d.cnki.gzhnu.2022.002978 (Central South University, 2022).
20. Li, Q. et al. Pulse permeability measurement and analysis of high temperature and high pressure unconventional reservoir. *J. China Coal Soc.* **47** (S1), 184–195. https://doi.org/10.13225/j.cnki.jccs.2020.1416 (2022).

21. Liu, J. Z., Gong, L. H., Bu, G. P. & Wu, X. High temperature and high pressure dynamic imbibition characteristics and influencing factors of tight sandstone reservoirs. *Spec. Oil Gas Reserv.* **28**(04):142–149. https://doi.org/10.3969/j.issn.1006-6535.2021.04.020 (2021).
22. Zhao, P. *Study on Seepage and Deformation Characteristics of Coarse-Grained Granite Under High Temperature Triaxial Stress* (Taiyuan University of Technology, 2021). https://doi.org/10.27352/d.cnki.gylgu.2020.001576
23. Zhao, P., Feng, Z. J., Nan, H. M. & Li, J. Dynamic shear-seepage characteristics of large displacement fractures in dry-hot granite rock mass. *J. China Coal Soc.* **48** (03), 1139–1154. https://doi.org/10.13225/j.cnki.jccs.2023.0124 (2023).
24. Wu, Z. S., Feng, Z. J., Zhang, C., Shi, X. D. & Hui, Z. Study on permeability variation of granite and backfill under two effective stresses. *J. Undergr. Sp. Eng.* **17** (05), 1391–1398 (2021).
25. Marco, F., MC, R. & Martin, S. Permeability evolution of Bentheim sandstone at simulated georeservoir conditions. *Sci. Rep.* **13** (1), 16171–16171 (2023).
26. Yin, W. T., Zhao, Y. S. & Feng, Z. J. Experimental study on permeability characteristics of post-fissure filled granite under high temperature triaxial stress. *Chin. J. Rock Mech. Eng.* **39** (11), 2234–2243. https://doi.org/10.13722/j.cnki.jrme.2020.0491 (2020).
27. Wu, J. W., Feng, Z. J., Liang, D. & Bao, X. K. Study on failure characteristics of high temperature steam injection of drilled granite under uniaxial stress. *Rock. Soil. Mech.* **40** (07), 2637–2644. https://doi.org/10.16285/j.rsm.2018.0488 (2019).
28. Domenico, L. R. P. & Andrew, C. The influence of grain shape and size on the relationship between porosity and permeability in sandstone: a digital approach. *Sci. Rep.* **12** (1), 7531–7531 (2022).
29. Li, S. et al. Permeability regain and aqueous phase migration during hydraulic fracturing shut-ins. *Sci. Rep.* **9**(1), 1–10 (2019).
30. Brace, W. F., Walsh, J. B. & Frangos, W. T. Permeability of granite under high pressure. *J. Geophys. Res.* **73** (6), 2225–2236. https://doi.org/10.1029/JB073i006p02225 (1968).
31. Jones, S. C. A technique for faster pulse-decay permeability measurements in tight rocks. *SPE Form. Eval.* **12** (1), 19–26. https://doi.org/10.2118/28450-PA (1997).
32. Dong, F. K. Study on the migration rule of pollutants in in-situ injection thermal mining of oil shale. (Taiyuan University of Technology, 2021). https://doi.org/10.27352/d.cnki.gylgu.2019.000050

Acknowledgements

This work is financially supported by the Hebei Province Education Department project (no. ZC2021014). The authors gratefully acknowledge financial support of the above-mentioned agencies.

Author contributions

Jieqing Yu, Fuke Dong and Yu Zhou wrote the main manuscript text and Xingyan Wang, Liang Zhang and Hailong Su prepared figures. All authors reviewed the manuscript.

Declarations

Competing interests

The authors declare no competing interests.

Additional information

Correspondence and requests for materials should be addressed to F.D.

Reprints and permissions information is available at www.nature.com/reprints.

Publisher's note Springer Nature remains neutral with regard to jurisdictional claims in published maps and institutional affiliations.